Magnetic Resonance in Medicine 51:140–147 (2004)

Visualization and Analysis of White Matter Structural Asymmetry in Diffusion Tensor MRI Data

Song Zhang,[1] Mark E. Bastin,[2*] David H. Laidlaw,[1] Saurabh Sinha,[3] Paul A. Armitage,[3] and Thomas S. Deisboeck[4,5]

This work presents a method that permits the characterization, quantification, and 3D visualization of white matter structural information contained within diffusion tensor MR imaging (DT-MRI) data. In this method, regions within the brain are defined as possessing linear, planar, or spherical diffusion. Visualization of this diffusion metric data is realized by generating streamtube and streamsurface models to represent regions of linear and planar diffusion. Quantification of differences in diffusion anisotropy between different regions of interest (ROIs) is then achieved by analyzing 2D barycentric histograms created from the complete distribution of diffusion metric values measured in each region. In four healthy volunteers, there was only a small degree of asymmetry (ε) in the number of linear, planar, or spherical diffusion voxels between the right and left hemispheres ($\varepsilon \simeq \pm 2\%$). However, in a patient with a metastatic brain lesion there was marked asymmetry in both linear ($\varepsilon \simeq -10\%$) and planar ($\varepsilon \simeq 5\%$) diffusion between comparable ipsilateral and contralateral regions, with a significant reduction in the number of linear diffusion voxels and an increase in the number of planar diffusion voxels in the tumor-bearing hemisphere. These results demonstrate the potential of this approach to characterize brain structure in both healthy and diseased subjects. Magn Reson Med 51:140–147, 2004.

Key words: brain; magnetic resonance imaging; diffusion; tensor; tumor

Diffusion tensor MR imaging (DT-MRI) allows the spatial mapping of the apparent diffusion tensor of water (D) in the brain (1). Diagonalizing D produces eigenvalues and eigenvectors, the effective principal diffusivities along the orthotropic axes of the tissue, which can be used to measure the mean diffusivity ($\langle D \rangle$) and diffusion anisotropy indices, such as the fractional anisotropy (FA) (2). Values of $\langle D \rangle$ indicate the magnitude of water molecule diffusion, while FA provides a scalar measure of diffusion anisotropy, which is the deviation from pure isotropic diffusion of water mobility in vivo.

While measuring the $\langle D \rangle$ and FA values of different parenchymal structures is important in characterizing the imaging signatures of healthy and diseased brain, a more complete understanding of anatomical connectivity and how it is altered in various pathologies requires the underlying white matter structure to be accurately mapped. This 3D tracking of white matter fiber bundles can be achieved using the information contained within the eigenvectors of D if it is assumed that the eigenvector associated with the largest principal diffusivity (eigenvalue) lies parallel to the local fiber tract direction (3). Although tracking the potentially tortuous 3D path of the principal eigenvector direction through many contiguous slices is not straightforward, a number of different approaches to this problem have recently been suggested (4). These methods allow the topology of major white matter fiber tracts, such as the corpus callosum, the internal and external capsules, and the pyramidal tract, to be determined.

One particularly interesting clinical application of these visualization techniques is in the study of intracranial tumors and how they affect surrounding brain structure. Several groups have already studied patterns of white matter tract disruption adjacent to brain tumors using DT-MRI data. Wieshmann et al. (5) found evidence of displacement of white matter fibers of the corona radiata in a patient with low-grade glioma when compared with spatially normalized data collected from 20 healthy volunteers. The data obtained from this particular patient were consistent with displacement rather than destruction of fibers due to the mass effect of the tumor. Mori et al. (6) found evidence of displacement and destruction of the superior longitudinal fasciculus and corona radiata in two patients with anaplastic astrocytoma. Gossl et al. (7) observed distortion of the pyramidal tract in a patient with a high-grade glioma. Finally, Witwer et al. (8) found evidence of white matter tract edema, infiltration, displacement, and disruption in 10 tumor patients with a range of brain malignancies. These studies show that while mapping white matter fiber tract disruption patterns in neoplasia is technically possible, more work is still required to validate DT-MRI tractography methods if they are to become a reliable tool for investigating brain structure and the pathophysiology of disease. Achieving this goal will require the development of robust protocols for measuring white matter tract topology, quantifying the natural biological variation in tract orientation in normal brain, and

[1]Department of Computer Science, Brown University, Providence, Rhode Island.

[2]Medical and Radiological Sciences (Medical Physics), University of Edinburgh, Edinburgh, UK.

[3]Clinical Neurosciences, University of Edinburgh, Edinburgh, UK.

[4]Complex Biosystems Modeling Laboratory, Harvard-MIT (HST) Athinoula A. Martinos Center for Biomedical Imaging, HST-Biomedical Engineering Center, MIT, Cambridge, Massachusetts.

[5]Molecular Neuro-Oncology Laboratory, MGH, Harvard Medical School, Cambridge, Massachasetts.

Grant sponsor: National Institutes of Health; Grant number: CA69246; Grant sponsor: Human Brain Project (NIDA, NIMH, NIB); Grant sponsor: National Science Foundation; Grant numbers: CCR-0086065; CCR-0093238; EIA-9724347; Grant sponsors: Cunningham Trust; William Ramsay Henderson Trust Scholarship; Scottish Hospital Endowments Research Trust.

S. Zhang and M.E. Bastin contributed equally to this work.

*Correspondence to: Dr. Mark E. Bastin, Medical and Radiological Sciences (Medical Physics), University of Edinburgh, Western General Hospital, Crewe Road, Edinburgh, EH4 2XU, UK. E-mail: meb@skull.dcn.ed.ac.uk

Received 22 May 2003; revised 9 September 2003; accepted 9 September 2003.

DOI 10.1002/mrm.10673
Published online in Wiley InterScience (www.interscience.wiley.com).

applying these analyses to carefully characterized patient groups.

As a first step toward developing such robust protocols, this work describes a method that permits the 3D visualization and quantification of the diffusion anisotropy information contained within DT-MRI data. In this method, regions within the brain are defined as possessing linear, planar, or spherical (isotropic) diffusion, based on the geometric properties of D (9). Visualization of these diffusion metrics is realized by generating streamtube and streamsurface models to represent regions of linear and planar diffusion (10). Quantification of differences in diffusion anisotropy between regions-of-interest (ROIs) is then achieved by analyzing 2D barycentric histograms created from the complete distribution of diffusion metric values measured in each region (11,12). Here the feasibility of using this approach in mapping normal brain structure and characterizing how neoplasia alters this structure is investigated.

MATERIALS AND METHODS

Subjects

To investigate the practicability of this method, five subjects were scanned. The first four subjects (two right-handed males, 43 years old; and two right-handed females, 26 and 33 years old) were normal healthy volunteers, while the fifth was a 72-year-old, right-handed male patient with a histologically confirmed right parietal solitary brain metastasis of a lung adenocarcinoma. The four volunteers were scanned to provide an estimate of the degree of asymmetry in diffusion metrics between cerebral hemispheres in normal brain. The fourth volunteer was also scanned on three separate occasions spread equally over three weeks to determine the reproducibility of the method. The ethics committee of the University of Edinburgh approved the study, and informed written consent was obtained from all subjects.

Data Acquisition

All MRI data were obtained using a GE Signa LX 1.5 T (General Electric, Milwaukee, WI) clinical scanner, equipped with a self-shielding gradient set (23 mT m^{-1} maximum gradient strength, 120 T m^{-1} s^{-1} slew rate, and 60-cm inner diameter horizontal bore) and a manufacturer-supplied birdcage quadrature head coil. The component diffusion-weighted (DW) images of the DT-MRI data set were acquired using a single-shot, spin-echo, echo-planar imaging (EPI) sequence in which two symmetric trapezoidal gradient pulses were inserted around the 180° refocusing pulse in the required gradient channel. Sets of coronal DW-EP images (b = 0 and 1000 s mm^{-2}) were collected with diffusion gradients applied sequentially along six noncollinear directions (13). Six acquisitions consisting of a baseline T_2-weighted EP image (G^0) and six DW-EP images (G^1–G^6), for a total of 42 images, were collected per slice position. Parameters for the DW-EPI sequence included a repetition time (TR) of 15 s, an echo time (TE) of 102.5 ms, a field of view (FOV) of 200 × 200 mm, an acquisition matrix of 128 × 128 (zero-filled to 256 × 256), and 36 contiguous coronal slices of 5-mm thickness. Therefore, each voxel had dimensions of 0.78 × 0.78 × 5.0 mm, with an inherent voxel resolution of 1.56 × 1.56 × 5.0 mm.

Bulk patient motion and eddy current-induced artifacts were then removed from the component EP images using a 3D computational image alignment technique (14). First, EP images with the same b-matrix were rigidly aligned to remove patient motion. Second, affine transformations were used to align the DW-EP images acquired with diffusion gradient directions G^2–G^6 to the first gradient direction G^1. Third, all DW-EP images were aligned using affine transformations to the T_2-weighted (G^0) acquisition. Then the set of six component EP images for each gradient direction was averaged to give seven high signal-to-noise ratio (SNR) images for each slice. Finally, from this MRI data D was calculated in each voxel from the signal intensities in the component EP images (1).

Diffusion Metrics

If $\lambda_1 \geq \lambda_2 \geq \lambda_3 \geq 0$ are the eigenvalues of the symmetric second-order diffusion tensor D, then diffusion can be considered linear (c_l: $\lambda_1 \gg \lambda_2 \approx \lambda_3$), planar ($c_p$: $\lambda_1 \approx \lambda_2 \gg \lambda_3$), or spherical ($c_s$: $\lambda_1 \approx \lambda_2 \approx \lambda_3$) depending on the values of $\lambda_{i\,=\,1,2,3}$ (9). For each voxel the relative magnitude of linear, planar, and spherical diffusion can be determined based on the values of

$$c_l = \frac{\lambda_1 - \lambda_2}{(\lambda_1 + \lambda_2 + \lambda_3)} \quad [1]$$

$$c_p = \frac{2(\lambda_2 - \lambda_3)}{(\lambda_1 + \lambda_2 + \lambda_3)} \quad [2]$$

and

$$c_s = \frac{3\lambda_3}{(\lambda_1 + \lambda_2 + \lambda_3)} \quad [3]$$

The factors 3 and 2 in c_s and c_p, coupled with the normalization factor ($\lambda_1 + \lambda_2 + \lambda_3 = Tr\{D\}$), imply that $[c_l, c_p, c_s] \in [0, 1]$, and $c_l + c_p + c_s = 1$. As discussed below, these metrics provide a means of visualizing, characterizing, and quantifying diffusion anisotropy in healthy and diseased brain.

Streamtubes and Streamsurfaces

The 3D information contained within D was visualized by identifying regions of linear and planar diffusion and representing them as red streamtubes and green streamsurfaces, respectively (15,16). Streamtubes, which represent coherent white matter tracts, are thin tubes that extend from seed points following the direction of fastest diffusion λ_1. This direction is only meaningful in regions of relatively high linear diffusion, so streamtubes were only created in such regions. The process for obtaining a small but representative set of streamtubes involved choosing the seed points, generating the streamtubes, and then culling them. Initially, a dense set of seed points was selected in the volume so as to cover as many interesting features as

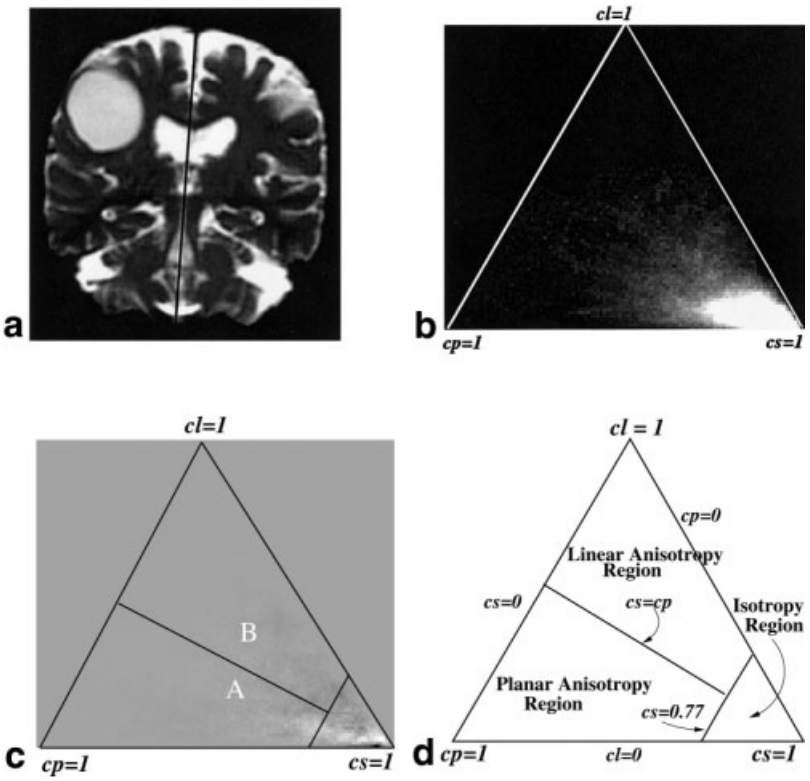

FIG. 1. The process of creating 2D barycentric histograms from DT-MRI data. **a:** For a given slice, the brain is divided in half with a straight line following the falx cerebri on the T_2-weighted EP image. **b:** A barycentric histogram is generated for each side of the brain. In this example, the histogram comes from the tumor-bearing section shown in **a.** Note the large number of voxels near the $c_s = 1$ vertex, reflecting the cystic component of the tumor. **c:** The difference histogram obtained by subtracting normalized barycentric histograms calculated from tumor-bearing and contralateral sections. In this difference histogram, zero maps to medium gray because the difference is signed. Note that the most striking difference occurs near the $c_s = 1$ vertex. **d:** The definition of the diffusion anisotropy regions in the barycentric histogram. These regions are chosen to capture the differences between regions A and B in part **c.**

possible. Each streamtube followed the local direction of λ_1, but was terminated when a region of low linear diffusion ($c_l < 0.2$) was encountered or the data boundary was reached. However, the resulting number of streamtubes was still considerable. For example, in a $256 \times 256 \times 36$ volume, more than 500000 streamtubes were produced by setting a seed point in every c_l voxel. Some of the streamtubes ran very close to others, while some were very short and were likely the result of noise contamination. A culling algorithm was therefore used to pick a representative subset (16). The culling criteria used included the length of the streamtube, the average diffusion anisotropy along the stream tube, and its similarity to other streamtubes. The streamsurfaces, which represent structures in regions of planar diffusion, were also generated and culled in this way. Finally, color was added to these geometric models to indicate the degree of linear or planar diffusion, with more saturated colors representing higher diffusion anisotropy values.

Barycentric Space Histograms

The three diffusion metrics can also be employed to quantify diffusion anisotropy in different brain regions using a barycentric space histogram approach (11,12). In this method a 2D triangular barycentric space containing all possible diffusion anisotropy values is defined, with c_l, c_p, and c_s being the barycentric coordinates. Asymmetries in the distribution of diffusion anisotropy values between the right and left hemispheres can then be characterized by

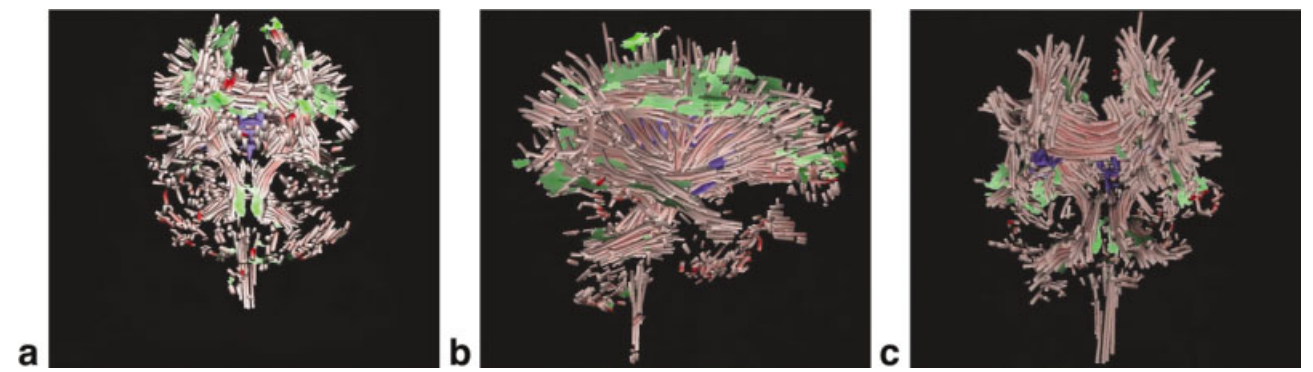

FIG. 2. Geometric models representing the diffusion metric data obtained from a 33-year-old female volunteer viewed from the (**a**) anterior, (**b**) right lateral, and (**c**) posterior directions. Linear diffusion is represented by red streamtubes, planar diffusion by green streamsurface fragments, and CSF by the blue surface.

Table 1
Comparison of Diffusion Metric Data Obtained From Right and Left Hemispheres for Four Normal Healthy Volunteers

	Volunteer 1 (male/43)			Volunteer 2 (male/43)			Volunteer 3 (female/26)			Volunteer 4 (female/33)			Mean ± SD	
Number (× 1000)	Right	Left	ε (%)	Right	Left	ε (%)	Right	Left	ε (%)	Right	Left	ε (%)	ε (%)	
Linear	459.84	459.45	0.04	623.60	597.47	2.14	407.85	390.49	2.17	526.12	551.75	−2.38	0.49 ± 2.16	
Planar	956.96	956.41	0.03	1,221.74	1,262.98	−1.66	952.51	997.77	−2.32	1,003.63	1,045.22	−2.03	−1.50 ± 1.05	
Spherical	3,352.18	3,308.82	0.65	3,507.74	3,355.15	2.22	3,148.14	3,056.85	1.47	3,371.16	3,378.21	−0.10	1.06 ± 1.01	
Percentage	Right	Left		Right	Left		Right	Left		Right	Left		Right	Left
Linear	9.6	9.7		11.7	11.5		9.0	8.8		10.7	11.1		10.3 ± 1.2	10.3 ± 1.3
Planar	20.1	20.2		22.8	24.2		21.1	22.4		20.5	21.0		21.1 ± 1.2	22.0 ± 1.8
Spherical	70.3	70.0		65.5	64.3		69.8	68.8		68.8	67.9		68.6 ± 2.2	67.8 ± 2.5

The percentage right/left asymmetry factor ε is defined in Eq. [4].

analyzing the barycentric histograms obtained from each side of the brain. Using data from the tumor patient, Fig. 1 illustrates how this process was implemented. First, for a given slice the brain was divided in half with a straight line following the falx cerebri on the T_2-weighted EP image coregistered with the DT-MRI data (Fig. 1a). A barycentric histogram was then generated for each side of the brain using the T_2-weighted EP image to identify voxels that were located within the cerebrum (Fig. 1b). To eliminate the effect of size differences between the two ROIs, the histograms were normalized so that the sum of all values within them was unity. The histograms were then subtracted to show how the two sides of the brain differ in diffusion anisotropy (Fig. 1c). Regions of linear, planar, and spherical diffusion within the 2D barycentric space were then defined. In order to capture the differences between regions A and B in the difference histogram close to the $c_s = 1$ apex (Fig. 1c), the isotropic region was defined as $c_s > 0.77$. The remaining space was split along the $c_l = c_p$ line. Thus, linear diffusion was defined as $c_s < 0.77$ and $c_l > c_p$, while planar diffusion was defined as $c_s < 0.77$ and $c_l < c_p$ (Fig. 1d). The number of voxels that fell within each of these regions was determined for a given number of slices for both sides of the brain to provide a 3D analysis. In the case of the four healthy volunteers, the slices chosen covered the entire cerebrum. However, for the tumor patient the analysis was performed not only for all slices covering the cerebrum, but also on just those slices in which signal hyperintensity was visible on the coregistered T_2-weighted EP images (i.e., the tumor/edema volume). To quantify the degree of asymmetry in the number of c_l (nc_l), c_p (nc_p), and c_s (nc_s) voxels in each ROI between the right and left sides of the brain, an asymmetry index (ε) of the form

$$\varepsilon(nc_l, nc_p, nc_s) = 100\,\frac{\text{right}(nc_l, nc_p, nc_s) - \text{left}(nc_l, nc_p, nc_s)}{\text{right}(nc_l, nc_p, nc_s) + \text{left}(nc_l, nc_p, nc_s)} \quad [4]$$

was evaluated (17). Finally, the percentage of voxels for each ROI characterized as possessing linear, planar, or spherical diffusion was determined.

RESULTS

Figure 2 displays a set of geometric models representing the diffusion metric data obtained from volunteer 4, a 33-year-old female, viewed from the (a) anterior, (b) right lateral, and (c) posterior directions. In this figures the red streamtubes represent structures characterized by linear diffusion, The green streamsurface fragments represent structures characterized by planar diffusion, and the blue surface represents structures that are hyperintense on the coregistered T_2-weighted EP images, namely cerebrospinal fluid (CSF) in the ventricles. (Note that the colors in these figures should not be confused with the standard color scheme used to represent the direction of the principal eigenvector of D in two dimensions.) The red streamtubes follow a number of major white matter fiber tracts (e.g., the corpus callosum, internal capsule, corona radiata, and op-

Table 2
Comparison of Diffusion Metric Data Obtained From Right and Left Hemispheres in a 33-Year-Old Female Volunteer Scanned on Three Separate Occasions

	First exam			Second exam			Third exam			Mean ± SD	
Number (× 1000)	Right	Left	ε (%)	Right	Left	ε (%)	Right	Left	ε (%)	ε (%)	
Linear	526.12	551.75	−2.38	513.92	521.88	−0.77	534.78	555.55	−1.91	−1.68 ± 0.83	
Planar	1,003.63	1,045.22	−2.03	970.85	1,007.61	−1.86	1,033.60	1,082.56	−2.31	−2.07 ± 0.23	
Spherical	3,371.16	3,378.21	−0.10	3,106.81	3,187.83	−1.29	3,388.47	3,266.30	1.84	0.15 ± 1.58	
Percentage	Right	Left		Right	Left		Right	Left		Right	Left
Linear	10.7	11.1		11.2	11.1		10.8	11.3		10.9 ± 0.3	11.2 ± 0.1
Planar	20.5	21.0		21.1	21.4		20.9	22.1		20.8 ± 0.3	21.5 ± 0.5
Spherical	68.8	67.9		67.7	67.6		68.4	66.6		68.3 ± 0.6	67.4 ± 0.7

tic radiations), while there are a number of small green streamsurfaces interspersed among them.

The results from the analysis of the 2D barycentric histograms obtained from the right and left hemispheres in the four normal volunteers are presented in Table 1. For all subjects the spherical diffusion class, which predominantly reflects gray matter and CSF, contains the greatest number of voxels (approximately 70% of all the voxels in the brain), while the linear diffusion class contains the fewest voxels (approximately 10% of all voxels). The planar diffusion class contains approximately 20% of all voxels. In these four volunteers there is very little asymmetry between the number of linear, planar, and spherical diffusion voxels found in each hemisphere, with ε varying between –2.38% and 2.22%. Furthermore, the average value of ε for the three diffusion classes is in the range of ±1.5%.

Table 2 displays the results of the analysis of the diffusion metric data obtained from volunteer 4 on three separate occasions. The values of ε for linear and especially planar diffusion voxels are reasonably reproducible, with ε being –2.38%, –0.77%, and –1.91 % for linear diffusion, and –2.03%, –1.86%, –2.31% for planar diffusion. Furthermore, the values for the percentage of voxels assigned to each diffusion class are very similar in the three examinations.

Figure 3 shows maps of (a) T_2-weighted signal intensity, (b) ⟨D⟩, (c) FA, and (d) color composite diffusion metric data for a coronal section through the tumor/edema volume in the 72-year-old male patient. Figure 4 presents a set of geometric models representing the diffusion metric data obtained from this patient viewed from the (a) anterior, (b) right lateral, and (c) posterior directions. In both these figures the growing metastasis, which probably originated at the gray/white matter junction of the brain, is clearly seen to affect the surrounding white matter fibers, thus altering the measured diffusion anisotropy. Figure 3c shows the total loss of white matter fiber structure within the tumor/edema volume, while Fig. 3d shows that the tumor/edema volume is surrounded by an extensive region of planar diffusion. This shell-like pattern in planar diffusion (green surface) surrounding the tumor/edema volume (yellow surface) is also evident in Fig. 4.

The results obtained from the analysis of the 2D barycentric histograms calculated for different-sized ROIs covering the ipsilateral and contralateral regions in this patient are shown in Table 3. The first set of three columns shows data obtained from an ROI covering both hemispheres, which is the ROI used in the volunteer studies above. The second set of three columns shows data obtained from an ROI formed from just those slices that cover the tumor/edema volume on the coregistered T_2-weighted EP images. For both ROIs there is a significant asymmetry between the number of linear and planar diffusion voxels identified in the ipsilateral and contralateral regions, and this asymmetry becomes more pronounced as the ROI becomes smaller. As suggested by Fig. 3d and 4, this asymmetry arises due to a reduction in the number of linear diffusion voxels and an increase in the number of planar diffusion voxels in the ipsilateral compared with the contralateral side of the brain. Thus, while the largest values of ε seen in the volunteer data sets is −2.38%, the effect of the tumor is to increase this right/left asymmetry to −8.35% for linear and 3.55% for planar diffusion. This asymmetry is even greater for the ROI formed from those slices that cover the tumor/edema volume, with ε being −13.05% for linear diffusion and 6.56% for planar diffusion.

DISCUSSION AND CONCLUSIONS

While there have been numerous studies reporting differences in cortical structure between the right and left hemispheres (18), asymmetries in white matter fiber tract connectivity are only beginning to be investigated. For example, Peled et al. (17) used line scan diffusion MRI to measure the asymmetry of a number of major white matter tracts in 24 healthy volunteers grouped according to sex and handedness. Employing the same diffusion metrics as used here, they found that while there were subtle differences in the diffusion anisotropy values of white matter fiber tracts between hemispheres, this asymmetry or laterality only became statistically significant in the anterior limb of the internal capsule, where c_l was greater in the right than in the left hemisphere. They also found that there was no significant dependence of asymmetry on sex or handedness. In the current study, diffusion metrics were obtained from large ROIs to highlight potential gross differences between healthy and diseased brain, which precluded an analysis of subtle differences in normal brain structure. Furthermore, since the measured reproducibility of the method (Table 2) is comparable to the asymmetry seen in the small group of volunteers (Table 1), no conclusions can be made here about whether there might be laterality in normal white matter fiber tract orientation. However, by considering large ROIs, the effect of neoplasia on normal brain structure becomes only too apparent.

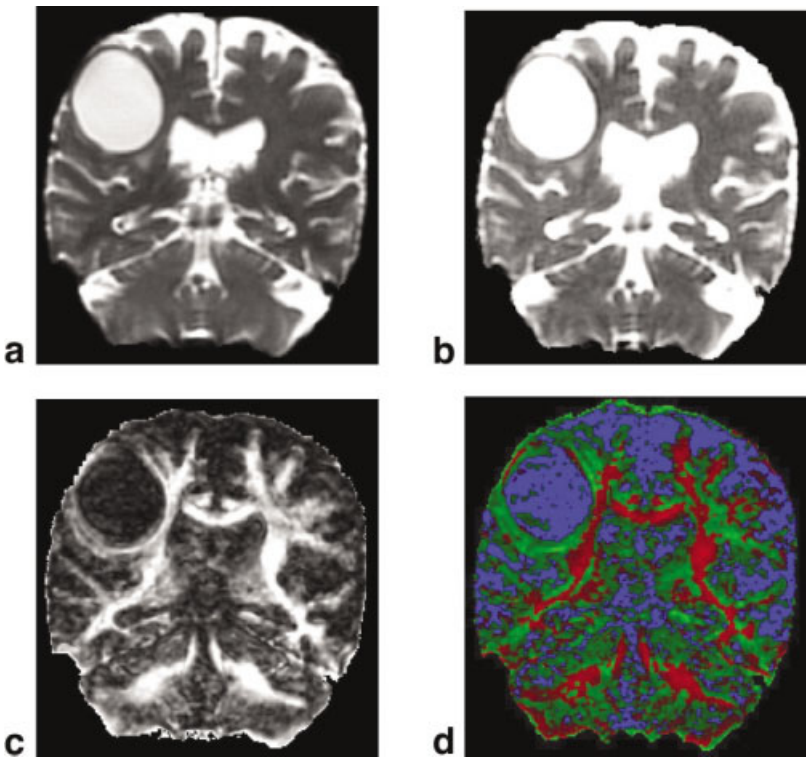

FIG. 3. Maps of (**a**) T_2-weighted signal intensity, (**b**) ⟨D⟩, (**c**) FA, and (**d**) color composite diffusion metric data obtained from a 72-year-old male patient with a right parietal metastasis of a lung adenocarcinoma. In **d**, maps of linear (red channel), planar (green), and spherical (blue) diffusion are overlaid so that the color in each voxel represents the relative magnitude of the three diffusion metrics. Note the high ⟨D⟩, low FA, and spherical (isotropic) diffusion of the tumor/edema volume. Also note that the tumor/edema volume is surrounded by a large region of planar diffusion.

While little asymmetry was measured between hemispheres in the volunteer group, in the brain tumor patient there was significant heterogeneity between ipsilateral and contralateral ROIs, with a marked reduction in linear diffusion and a significant increase in planar diffusion on the tumor-bearing side. In healthy brain, linear diffusion is associated with large, coherently organized white matter fiber tracts, such as commissural and deep projection (internal capsule and corticospinal) fibers. The cause of planar diffusion is less well understood, but such diffusion is thought to originate from tissue membranes arranged in sheets, crossing and twisting of white matter fibers, or partial volume averaging of gray and white matter tissue. The reduction in linear diffusion in the tumor-bearing hemisphere is therefore probably related to the loss of structural organization resulting from the combined effects of necrosis, tumor infiltration, and increased free water fraction (19). The increase in planar diffusion in peritumoral brain is interesting, and there are several possible explanations for this increase. For example, it could be argued that the expanding tumor leads to a rapidly growing peritumoral edema front that extends in the direction of least resistance. These paths of least resistance are anatomically predetermined, are not confined to the region of T_2-weighted hyperintensity, and include white matter fiber tracts and the perivascular space (20). If, however,

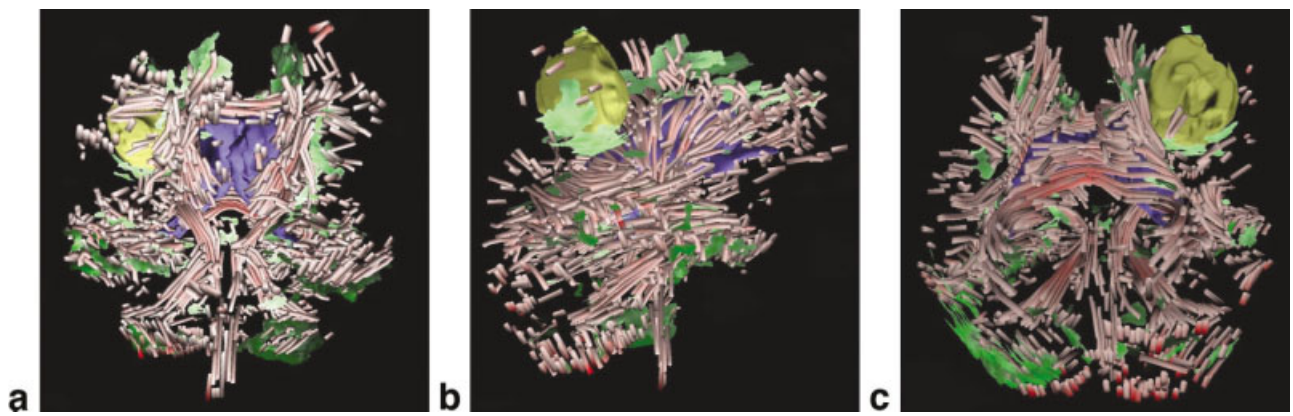

FIG. 4. Geometric models representing the diffusion metric data obtained from the 72-year-old male patient viewed from the (**a**) anterior, (**b**) right lateral, and (**c**) posterior directions. Linear diffusion is represented by red streamtubes, planar diffusion by green streamsurface fragments, and CSF by the blue surface. The yellow surface, which is rendered from the signal abnormality on the T_2-weighted EP images, depicts the shape of the tumor/edema volume. Note that the tumor/edema volume is partly surrounded by regions of planar diffusion.

Table 3
Comparison of Diffusion Metric Data Obtained From Different Sized Regions-of-Interest Covering Tumor/Edema (Ipsilateral) and Contralateral Volumes in a 72-Year-Old Male Patient With a Right Parietal Metastasis of a Lung Adenocarcinoma

	Hemisphere			Slices covering tumor/edema volume		
	Ipsilateral	Contralateral	ε (%)	Ipsilateral	Contralateral	ε (%)
Number ($\times$ 1000)						
Linear	392.04	463.48	−8.35	255.85	332.64	−13.05
Planar	1,164.38	1,084.59	3.55	722.63	633.67	6.56
Spherical	3,129.50	3,112.84	0.27	1,513.74	1,429.83	2.85
Percentage						
Linear	8.4	9.9	–	10.3	13.9	–
Planar	24.8	23.3	–	29.0	26.4	–
Spherical	66.8	66.8	–	60.7	59.7	–

edema production exceeds the draining capacity of these paths, edema fluid could be squeezed interstitially (i.e., perpendicular to the principal fiber direction), creating what is observed as planar diffusion. It is also conceivable that a majority of these planar structures may in fact depict crossing neural fibers that are forced into close proximity by the compression produced by the moving edema front or from partial volume averaging of linear and spherical diffusion voxels. Further work on larger patient populations is required to clarify these preliminary observations.

Although the current approach is promising, there are several points that require further discussion. As shown in Tables 1–3, the number of voxels in each diffusion metric class depends not only on the size of the ROI, but also on how the regions of linear, planar, and spherical diffusion are defined in the barycentric histograms. In this study, the thresholds for the three diffusion metric classes were chosen to highlight regions in the difference histograms derived from the tumor patient's imaging data, in order to emphasize structural differences between the peritumoral brain and the apparently normal brain. Since this patient's tumor has a large cystic component, which is characterized by isotropic diffusion (cf. Fig. 1b and 3c and d), the most pronounced difference between the barycentric histograms obtained from the tumor-bearing and contralateral hemispheres occurs near the $c_s = 1$ vertex (Fig. 1c). In order to capture this difference (as well as the differences in regions A and B, which also occur near this vertex), the spherical diffusion region was defined as $c_s > 0.77$. In tumors without such a large cystic component, and in other pathologies, it might be appropriate to change this threshold.

ROI definition also clearly affects the results presented above. For example, due to the presence of concentrated regions of high linear and planar diffusion along the falx cerebri, a relatively small positional change in the cutting line separating the right and left halves of the brain will affect the results of the histogram analysis and contribute to the small variation in diffusion metric values seen in the reproducibility experiment (Table 2). (It should also be noted that although the above results were obtained from large ROIs covering the right and left hemispheres, there is no technical reason why data obtained from smaller ROIs concentrated on specific anatomical structures could not be analyzed using this method, as long as these ROIs are appropriately defined (17).) Finally, the current voxel acquisition dimension (1.56 $\times$ 1.56 $\times$ 5 mm) may bias the diffusion anisotropy results in the out-of-plane (anterior/posterior) direction. This problem could be relatively easily addressed with the use of an acquisition that gives isotropic voxels (21). These points notwithstanding, the results presented above show that generating streamtube and streamsurface models of linear and planar diffusion combined with a quantitative analysis of the associated barycentric space histograms is a promising technique for visualizing and quantifying brain structure in both healthy and diseased subjects. Future work will therefore focus not only on investigating these issues, but also on extending the analysis to larger volunteer and patient groups.

ACKNOWLEDGMENTS

The current MRI studies were carried out at the SHEFC Brain Imaging Research Centre for Scotland, University of Edinburgh, UK (http://www.dcn.ed.ac.uk/bic). The authors thank Dr. E. Antonio Chiocca (MGH-Neurosurgical Service, Harvard Medical School) and Dr. Ian Marshall (University of Edinburgh) for useful discussions.

REFERENCES

1. Basser PJ, Mattiello J, LeBihan D. Estimation of the effective self-diffusion tensor from the NMR spin echo. J Magn Reson B 1994;103: 247–254.
2. Basser PJ. Inferring microstructural features and the physiological state of tissues from diffusion-weighted images. NMR Biomed 1995;8:333–344.
3. Basser PJ, Pajevic S, Pierpaoli C, Duda J, Aldroubi A. In vivo fiber tractography using DT-MRI data. Magn Reson Med 2000;44:625–632.
4. Ito R, Mori S, Melhem ER. Diffusion tensor brain imaging and tractography. Neuroimaging Clin N Am 2002;12:1–19.
5. Wieshmann UC, Symms MR, Parker GJ, Clark CA, Lemieux L, Barker GJ, Shorvon SD. Diffusion tensor imaging demonstrates deviation of fibres in normal appearing white matter adjacent to a brain tumour. J Neurol Neurosurg Psychiatry 2000;68:501–503.
6. Mori S, Frederiksen K, van Zijl PC, Stieltjes B, Kraut MA, Solaiyappan M, Pomper MG. Brain white matter anatomy of tumor patients evaluated with diffusion tensor imaging. Ann Neurol 2002;51:377–380.
7. Gossl C, Fahrmeir L, Putz B, Auer LM, Auer DP. Fiber tracking from DTI using linear state space models: detectability of the pyramidal tract. Neuroimage 2002;16:378–388.
8. Witwer BP, Moftakhar R, Hasan KM, Deshmukh P, Haughton V, Field A, Arfanakis K, Noyes J, Moritz CH, Meyerand ME, Rowley HA, Alexander AL, Badie B. Diffusion-tensor imaging of white matter tracts in patients with cerebral neoplasm. J Neurosurg 2002;97:568–575.

9. Westin C-F, Peled S, Gudbjartsson H, Kikinis R, Jolesz FA. Geometrical diffusion measures for MRI from tensor basis analysis. In: Proceedings of the 5th Annual Meeting of ISMRM, Vancouver, Canada, 1997; p 1742.
10. Westin CF, Maier SE, Mamata H, Nabavi A, Jolesz FA, Kikinis R. Processing and visualization for diffusion tensor MRI. Med Image Anal 2002;6:93–108.
11. Kindlmann GL, Weinstein DM. Hue-balls and lit-tensors for direct volume rendering of diffusion tensor fields. Proc IEEE Visualization 99 1999;99:183–190.
12. Alexander AL, Hasan K, Kindlmann G, Parker DL, Tsuruda JS. A geometric analysis of diffusion tensor measurements of the human brain. Magn Reson Med 2000;44:283–291.
13. Basser PJ, Pierpaoli C. A simplified method to measure the diffusion tensor from seven MR images. Magn Reson Med 1998;39:928–934.
14. Jenkinson M, Smith S. A global optimisation method for robust affine registration of brain images. Med Image Anal 2001;5:143–156.
15. Zhang S. Visualizing diffusion tensor MR image using streamtubes and streamsurfaces. Master's thesis, Brown University, Providence, Rhode Island, 2000.
16. Zhang S, Demiralp C, Laidlaw DH. Visualizing diffusion tensor MR images using streamtubes and streamsurfaces. IEEE Trans Vis Comput Graphics (In press)
17. Peled S, Gudbjartsson H, Westin CF, Kikinis R, Jolesz FA. Magnetic resonance imaging shows orientation and asymmetry of white matter fiber tracts. Brain Res 1998;780:27–33.
18. Galaburda AM, LeMay M, Kemper TL, Geschwind N. Right-left asymmetrics in the brain. Science 1978;199:852–856.
19. Sinha S, Bastin ME, Whittle IR, Wardlaw JM. Diffusion tensor MR imaging of high-grade cerebral gliomas. AJNR Am J Neuroradiol 2002; 23:520–527.
20. Geer CP, Grossman SA. Interstitial fluid flow along white matter tracts: a potentially important mechanism for the dissemination of primary brain tumors. J Neurooncol 1997;32:193– 201.
21. Jones DK, Williams SC, Gasston D, Horsfield MA, Simmons A, Howard R. Isotropic resolution diffusion tensor imaging with whole brain acquisition in a clinically acceptable time. Hum Brain Mapp 2002;15: 216–230.